Challenge Journal of Structural Mechanics

Bonded particles models of rock plates with circular cavities in uniaxial and biaxial compression

Michail A. Lotidis *, Pavlos P. Nomikos, Alexandros I. Sofianos

Tunnelling Laboratory, School of Mining and Metallurgical Engineering, National Technical University, GR-157 80 Athens, Greece

ABSTRACT

In this paper, a distinct elements code is used to perform a numerical investigation for the size and stress gradient effects on the fracture initiation and propagation around single or pairs of pre-existing cavities in brittle rock. To investigate the rock fracture around cavities and to assess the potential of the numerical model to simulate this behavior, published laboratory physical model on granite is simulated numerically with a Bonded Particles Model (BPM). The numerical model is presented and the calibration of the BPM micro-parameters is described. Then, the calibrated BPMs are used to investigate the effect of the size of the cavity on the primary, secondary and side wall fracturing, as well as on the fracturing modes. Moreover, BPMs with two circular cavities were used to study the interaction of these holes of the same diameter and to investigate the importance of their relative distance. Finally, the simulated material was studied by biaxial tests on BPMs with a pre-existing hole.

ARTICLE INFO

Article history:
Received 26 August 2016
Accepted 1 November 2016

Keywords:
Bonded particles model
Numerical simulation
Granite
Rock fracture

1. Introduction

Over the past decade, the Bonded Particles Model (BPM) (Potyondy and Cundal, 2004) has extensively been used in order to simulate the mechanical behavior and fracture of rock under a variety of loading configurations. In the BPM, the intact rock is represented by a dense packing of rigid spheres (in 3D) or disks (in 2D) bonded together at their contacts. The model is implemented in the Particle Flow Code (PFC) (Itasca, 2014). With the recent addition of the flat-joint contact logic in the BPM (Potyondy, 2012) particle interlocking and friction resistance at the contact are imposed, restricting the relative movement of particles, and thus attaining the advantages of simulating the rock structure.

In this study, the BPM is used to model the fracture initiation and damage around cylindrical openings in compression. Published laboratory physical model on granite (Carter et al., 1991) is simulated numerically with the PFC2D by using flat-joint contact model.

2. Calibration of the Numerical Models

The mechanical properties of the granite used for the physical model experiments (Carter et al., 1991) are shown in column 3 of Table 1. The Flat-Joint Model (Itasca, 2014) was used on the BPMs for the simulation of granite's specimens. The relevant micro-parameters are presented in Table 2. Column 5 of Table 1 shows the simulation results by using the micro-parameters of Table 2. A very good match of the numerically evaluated macro-properties with the experimental ones is observed.

Carter et al. (1991) performed unconfined uniaxial compression experiments on prismatic granite specimens with a circular hole of 3.6 mm. In order to reduce friction, two granite plates of 3cm thickness were placed by the researches between the platens of the compression machine and the specimen. According to their observations, primary tensile fractures originating from the top and bottom of the cavity were initially formed at an axial stress of 16 MPa. Stable propagation of these

* *Corresponding author*. Tel.: +30-210-7721671 ; E-mail address: mlotidis@metal.ntua.gr (M. A. Lotidis)
ISSN: 2149-8024 / DOI: http://dx.doi.org/10.20528/cjsmec.2016.11.026

cracks was the only phenomenon observed until the formation of remote fractures, away from the opening, at an axial stress of 119 MPa. These were followed by slabbing at the sides of the hole when the axial stress was about 126 MPa. These observations are summarized in column 2 of Table 3. The test described by Carter et al. (1991) was completed at 157MPa, without reaching the maximum strength, in order not to destruct the specimen completely. The investigators report that cracks are not readily apparent due to the nature of the rock.

Table 1. Mechanical properties of granite (Carter et al., 1991) and simulation results.

Mechanical Property	Value	Standard deviation	Simulation results
Tensile strength (Brazilian)	14 MPa	1.2 MPa	14.3 MPa
Uniaxial compressive strength	226 MPa	15 MPa	226 MPa
Young's modulus	71.3 GPa	4.7 GPa	70 GPa

Table 2. Micro-parameters of BPM for granite.

Micro-parameter	Value	Micro-parameter	Value
Disk radius (mm)	0.36 – 0.6	Tensile strength (MPa)	14.2
Contact modulus (GPa)	65	Cohesion (MPa)	98
Stiffness ratio	2.5	Friction coefficient	0.685

Table 3. Fracture initiation stress levels in prismatic granite specimens with a cylindrical hole subjected to uniaxial compression, as observed by Carter et al. (1991) and by the BPM of this study.

Fracture type	Stress (MPa)	Standard deviation (MPa)	Simulation results (MPa)
Primary	16	2.7	17
Remote	119	10	-
Slabbing	126	12	120

In the BPMs prepared with PFC2D, the aforementioned friction angle between the platens and the specimen was set zero as the implementation of such 3cm thick plates didn't result in any substantial differences (Lotidis, 2014; Lotidis et al., 2015). The UCS simulation results of the prismatic BPM with a 3.6cm diameter hole are shown in column 4 of Table 3.

During the simulation of the physical test, primary cracks initially formed above and below the hole, initiating from the top and bottom boundary and extending towards the upper and lower surfaces of the BPM, respectively. After the initiation of the two primary fractures, a micro-cracking observed away from the hole. In the course of the UCS test, the micro-cracking becomes more widespread but scattered within the model. The slabbing at the sides of the hole starts as soon as shear cracks occur on the area of high stress concentration (AHSC) of the boundary. Finally, there is a strong presence of shear macroscopic fracture surfaces (MFSs) joining the AHSCs of the bases of the model.

It may be observed from Table 3, that the axial stress of primary fractures appearance at the top and bottom of the hole and the slabbing axial stress of physical models and BPM are in very close agreement. Any difference arising from the BPMs with those of physical models is within the respective standard deviation referred to physical specimens. Also, in Fig. 1, the similarity of the fracture pattern of the BPM with the physical model of granite may be observed. Note that Fig. 1 illustrates the two models (physical and numerical respectively) during the same applied stress level, i.e. 157 MPa. Concerning the applied axial stress of remote fractures a safe parallelism of the BPM with the physical model may not be performed.

Afterwards, five BPMs were prepared with the parameters shown in Table 2 and dimensions 20 cm x 20 cm, each containing a single circular hole at the center with varying diameter (D) 1.0, 2.0, 3.0, 3.6 and 5.0 cm. The BPMs were subjected numerically to unconfined uniaxial compression and the applied axial stress where the first tensile and shear cracks appeared at the top/bottom and at the sides of the hole's boundary respectively, were measured. In addition, the applied axial stress during the initiation of slabbing and the maximum stress attained by each BPM were recorded. These results are plotted in Fig. 2, where the variation of the abovementioned stress levels with the hole's diameter is shown. BPM with 3.6cm hole's diameter was compared with Carter's physical model (red markers) which had the same dimensions.

The effect of the hole's diameter on the fracturing stress levels is observed from Fig. 2. The numerical models have similar behavior and cracking and failure mechanisms. Specifically, primary fractures initially formed above and below the hole, which initiate from the periphery of the hole and extending towards the upper and

lower surfaces of the model, respectively. After initiation of the two primary fractures, a micro-cracking observed away from the hole. In the course of the UCS test, the micro-cracking becomes more widespread but scattered within the model. Then, the micro-cracks coalescence and one may observe an increasing curvature on the mean axial stress-axial strain curves σ_α-ε_α (Fig. 1(b)). Slabbing starts as soon as shear cracks occur on the AHSCs of the boundaries. Finally, there is a strong presence of shear MFSs joining the AHSCs with the bases of the models. Moreover, the diagram of Fig. 2 shows that the compared values reduce as the diameter of the hole increases. In addition, axial stresses at which the 1st tensile cracks are observed are similar. Finally, common for the five BPMs is the fact that the first shear cracks occurred on the boundary of the hole, either from the left or from the right, with the slabbing of the holes lie in their presence.

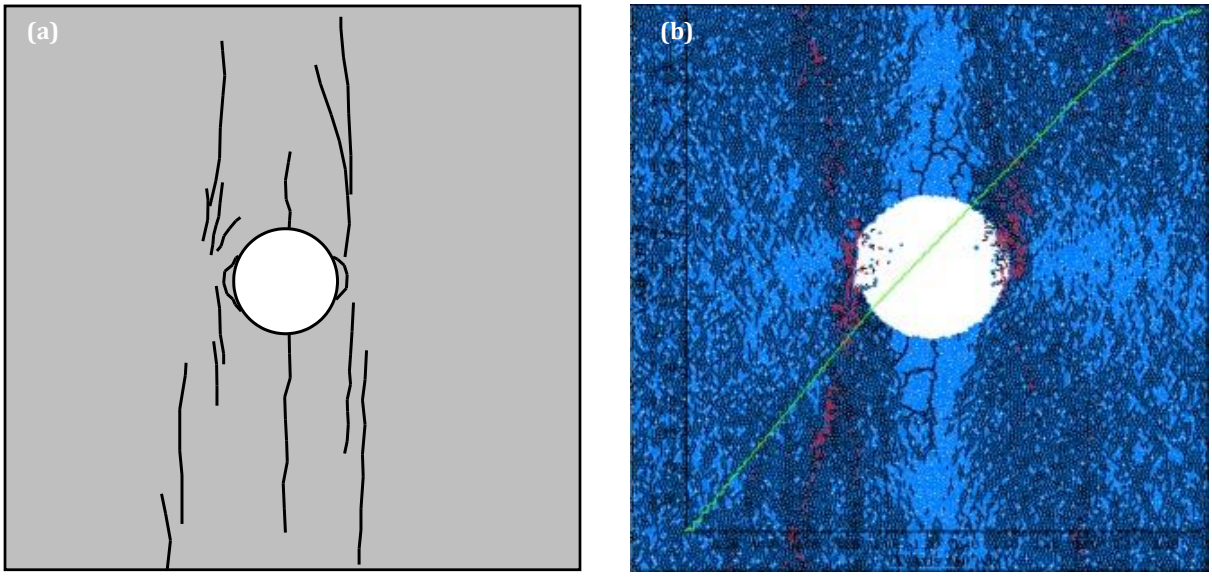

Fig. 1. Fracture pattern of: (a) granite specimen after UCS test (Carter et al. 1991) and (b) BPM micro-cracking (tensile cracks=black color, shear cracks=red color, stress-strain curve=green color, D=3.6 cm).

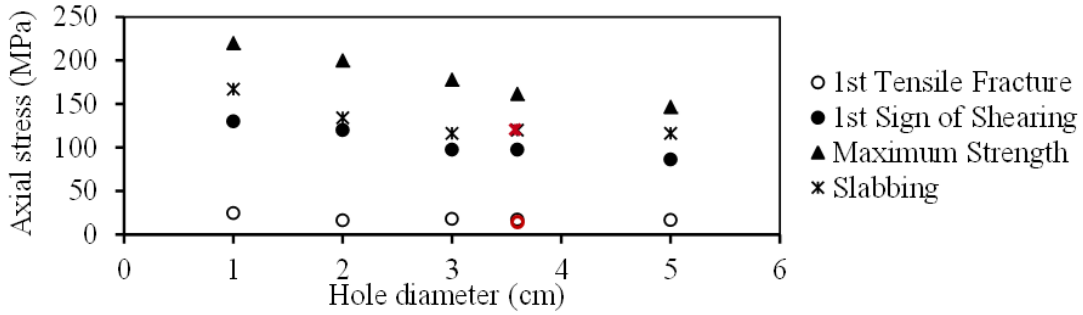

Fig. 2. Axial stress levels for 1st tensile crack/1st sign of shearing/slabbing/strength with respect to the hole's diameter, as measured from the BPMs of granite. Red markers represent the results of the physical models of Carter et al. (1991).

3. Pair of Circular Holes

The realistic results of the simulations of the previous paragraph encouraged the design of a new series of numerical models, using the micro-parameters of Table 2.

Five (5) BPMs were designed with dimensions 20 cm x 20 cm, each containing a pair of circular holes of 3cm diameter, with varying distance (X) between their centers and symmetrical relative to the center of the BPM, i.e. 4, 5, 7, 8 and 10 cm. The results of the aforementioned simulations are presented in Table 4, where the respective values of the BPM with a single circular hole of 3cm diameter are also shown. The comparative graph of Fig. 3 contains the simulation results on PFC2D for the granite BPMs with a pair of circular holes (D=3 cm). Vertical axis represents the applied axial stress (MPa) which was responsible for each phenomenon. Horizontal axis represents the distance (cm) between the holes' centers. L and R stand for "left" and "right" hole respectively.

The purpose of this test series was to study the interaction of two circular holes of equal diameter (D=3 cm) and the importance of the relative distance between them.

The UCS testing on the BPMs with a pair of holes shows similar cracking mechanism for all the numerical samples. Initially, tensile cracks are formed above and below the holes, which start from the boundary of each hole and extend to the upper and lower surfaces of the

model respectively. After the initiation of these cracks, there is some mixed-mode micro-cracking, i.e. appearance of tensile and shear cracks, away from the holes. During the progress of the UCS testing, this micro-cracking extends at an angle of 45° (with respect to the center of each hole) to four directions, tending to join the AHSCs. The MFSs with direction from the left opening to the right and from the right hole to the left extend to meet each other in the vertical axis of symmetry of the BPM, and as a result the numerical specimen tends to fail on the symmetry axis.

For the distance of 4 cm, the pillar between the two holes was collapsed, while the surfaces of cracks reached the underside of the model, in combination with the MFS on the vertical axis of symmetry at the top of the model, and as a result they separate the numerical model into three large pieces. The numerical model with 5 cm distance has a similar to the previous BPM failure mechanism, except that the pillar between the two holes didn't collapse. Finally, the holes of the three other numerical models with distances 7 cm, 8 cm and 10 cm tend to behave as independent.

Table 4. Comparative table of the simulation results on PFC2D for Lac du Bonnet granite BPMs with a single and pair of circular holes (D=3 cm).

D=3 cm	UCS (MPa)	Primary fracture (left hole) (MPa)	Primary fracture (right hole) (MPa)	Slabbing (left hole) (MPa)	Slabbing (right hole) (MPa)
Single	178	18	18	116	116
Pair X=4 cm	148	18	17.8	75.4 (right)	90 (left)
Pair X=5 cm	152	16	20	110 (right)	112 (right)
Pair X=7 cm	138	22	14.4	109 (right)	107 (right)
Pair X=8 cm	147.5	16.8	17.8	110 (right)	105 (left)
Pair X=10 cm	133	13.9	15.2	97 (left)	102 (right)

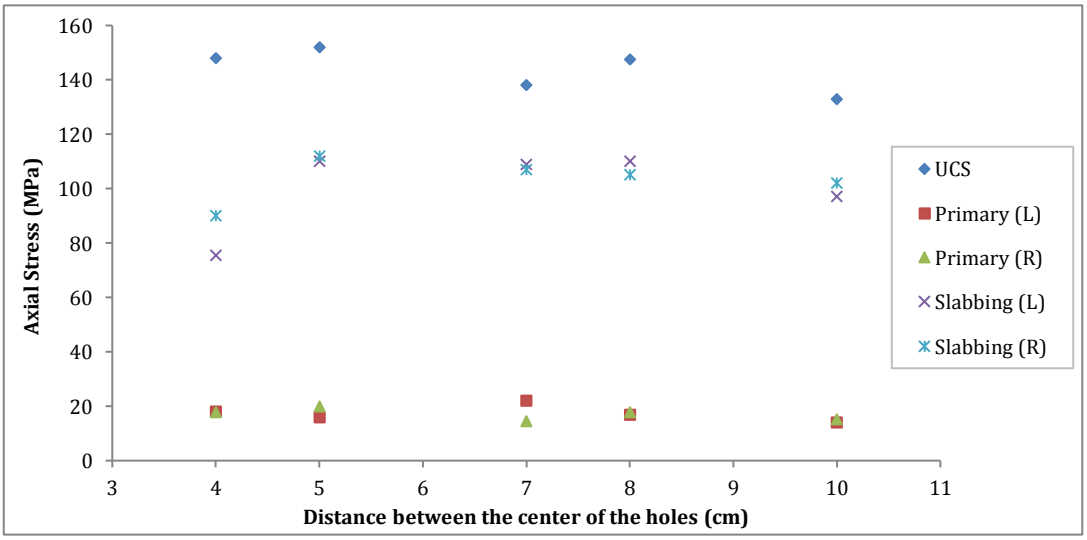

Fig. 3. Comparative graph of the simulation results on PFC2D for granite BPMs with a pair of circular holes (D=3 cm). Vertical axis represents the applied axial stress (MPa) which was responsible for each phenomenon. Horizontal axis represents the distance (cm) between the holes' centers. L and R stand for "left" and "right" hole respectively.

Observing the values (maximum strength/primary fracture on the left and right hole/slabbing of the left and right hole) of Table 4, it seems that the maximum strength of the numerical model decreases with the increasing distance between the two holes, while the initiation of the primary crack at the upper or lower boundary of the holes is observed at similar level of mean axial stress on the six BPMs. Moreover, on the first BPM (X=3 cm) as expected, the slabbing begins from the right of the left hole and from the left of the right hole due to the high stress concentration stress distribution through the pillar.

The fracture patterns obtained from UCS testing on PFC2D of granite BPMs with a pair of circular holes (D=3 cm) are given below in Fig. 4. The green curves represent the applied axial stress vs the axial strain (σ_α-$E_{\varepsilon\alpha}$). Disks with different color than blue represent fragments.

4. Biaxial Test

The last simulation series of this study contains biaxial compressive tests on PFC2D, by using the BPM that was designed for the simulation of the physical experiment of Carter et al. (1991), i.e. 20cm x 20cm and D=3 cm. Four (4) biaxial tests took place with different lateral stress p, i.e. 2, 5, 10 and 20 MPa, following the same methodology: first, the BPM is submitted into increasing hydrostatic stress field beginning from 0 MPa until $\sigma_1 = \sigma_3 = p$. Then, the lateral stress remains constant ($\sigma_3 = p$) within an approximate error equal to 0.05%, and the applied axial stress (σ_1) increases until the collapse of the BPM.

The concept of the fracture process and mechanism for the biaxial tests stays the same as for the UCS test of paragraph No 2. Noteworthy is the micro-cracking initiation when $p \geq 5$ MPa, as the first micro-cracks are nucleated either at the left or the right of the boundary of the hole, instead of the upper or lower, i.e. primary fractures. In addition, during the biaxial tests, shear micro-cracking becomes more intense than the UCS test, leading on the creation of small fragments along the MFSs. The size of these fragments decreases as the lateral stress increases. They start from the four (4) MFSs and they pullulate as the axial stress σ_1 increases.

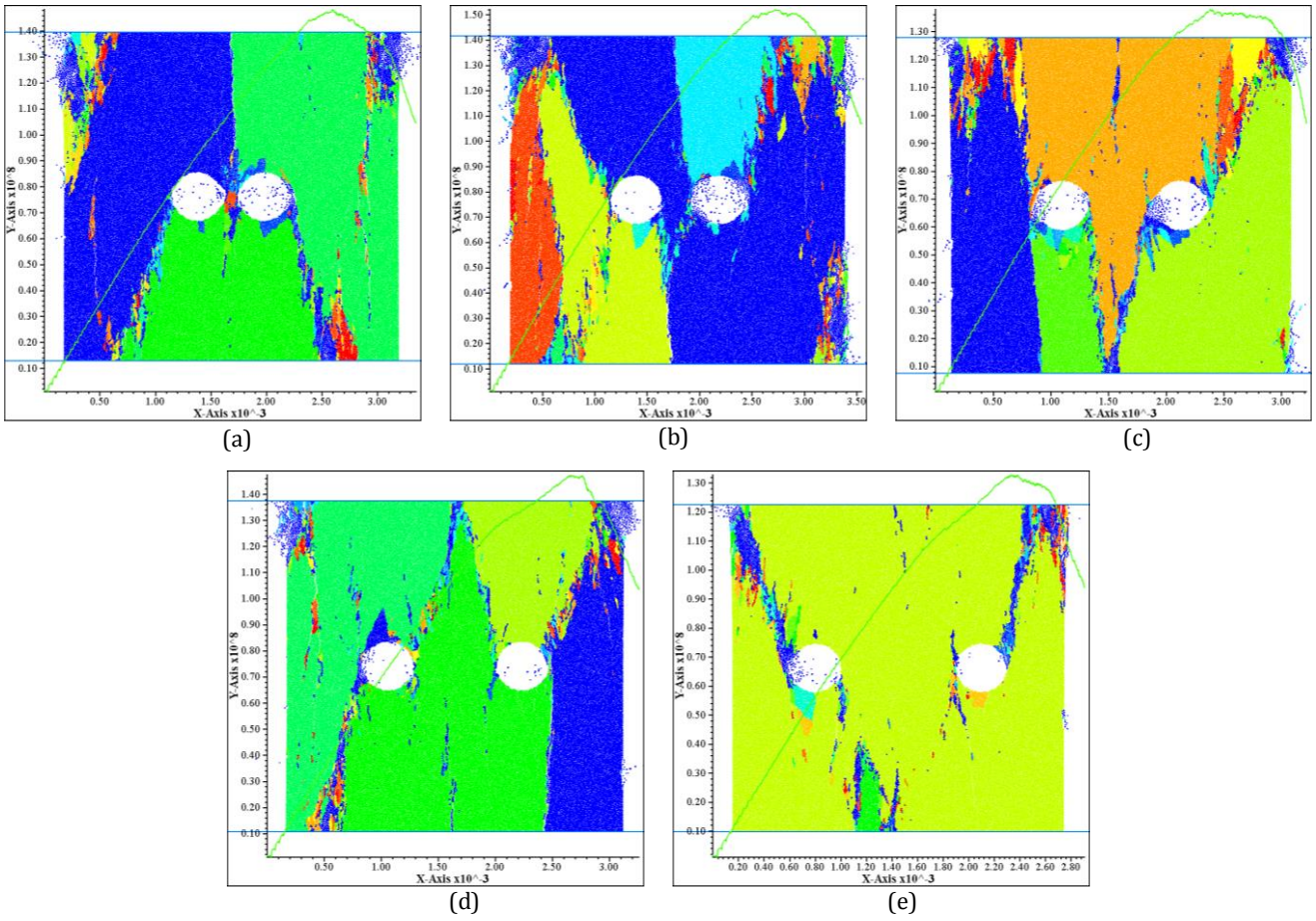

Fig. 4. BPMs of granite with a pair of holes (D=3 cm) after the UCS testing on PFC2D. Disks with different color than blue represent fragments. (a) X=4 cm; (b) X=5 cm; (c) X=7 cm; (d) X=8 cm; (e) X=10 cm.

Fig. 5 presents the simulation results in comparison with the UCS values of the same BPM. Blue, red, green, purple and light blue markers represent the maximum strength of the BPM, the primary fracture initiation, the slabbing initiation and the total length of the upper and the lower primary fracture respectively. As one may observe, the total length of the primary fractures decreases as the lateral stress increases. On the other hand, the maximum strength and the applied axial stress for the primary fracture initiation increase. In this series, slabbing initiation occurs on higher stress levels than the UCS test, but it remains on the same magnitude for each biaxial test.

The fracture patterns obtained from biaxial testing on PFC2D of granite BPM with a circular hole (D=3.6 cm) are given in Fig. 6. The green curves represent the applied axial stress vs the volumetric strain (σ_α-ε_{vol}). Disks with different color than blue represent fragments.

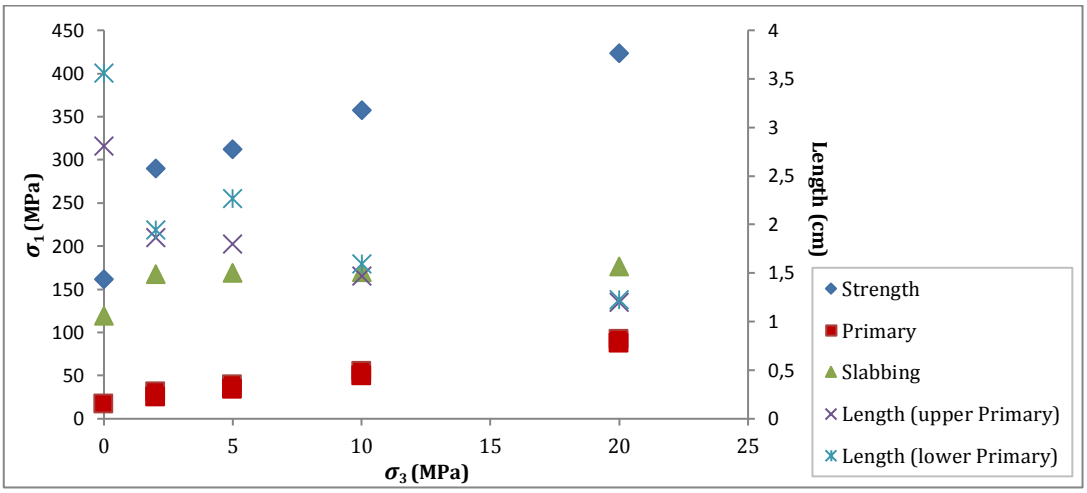

Fig. 5. Simulation results of biaxial tests on PFC2D for BPM of granite. Blue, red, green, purple and light blue values represent the maximum strength of the BPM, the primary fracture initiation, the slabbing initiation and the total length of the upper and the lower primary fracture respectively.

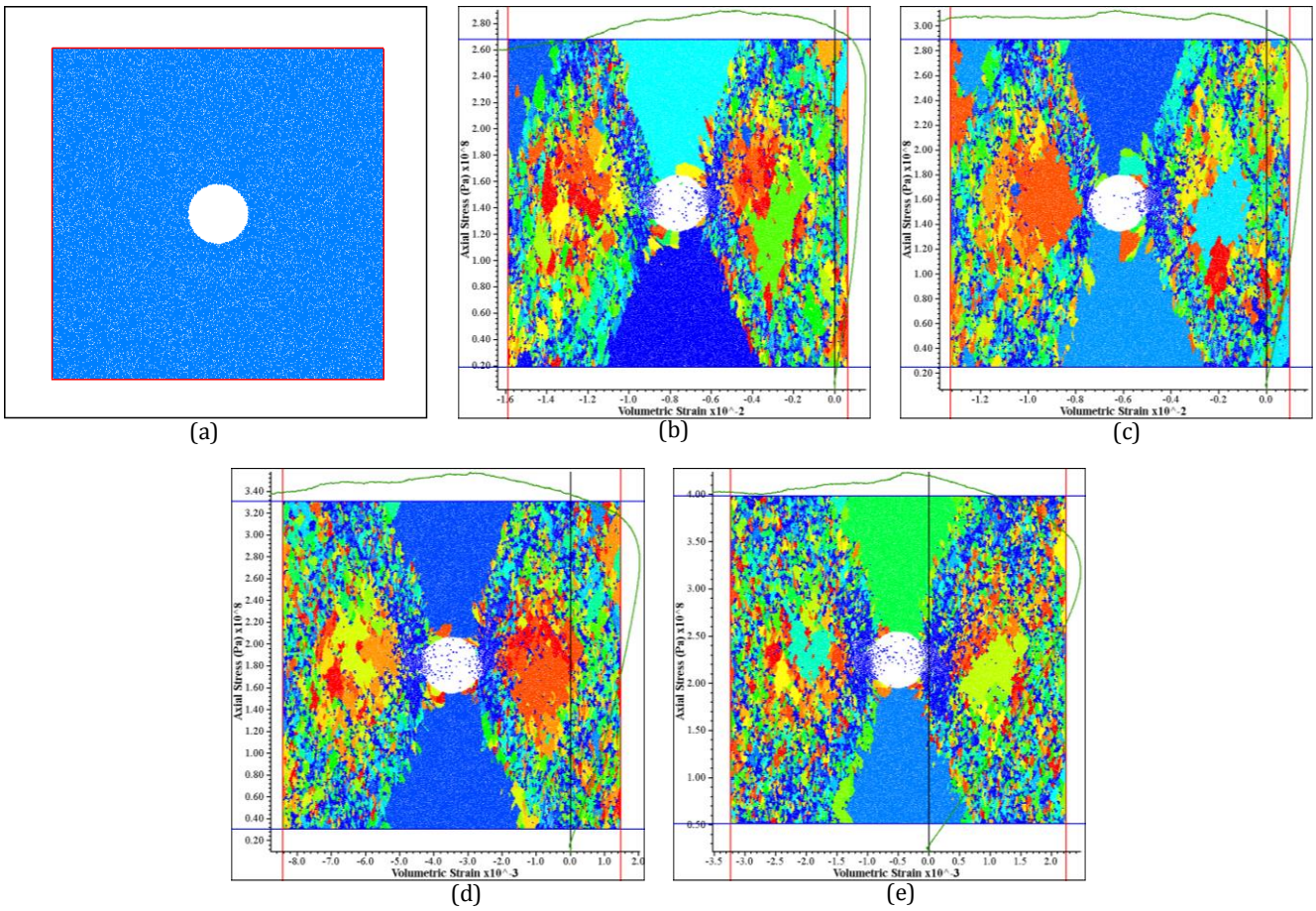

Fig. 6. BPM of granite with a single hole (D= 3.6 cm) after the biaxial testing on PFC2D. Disks with different color than blue represent fragments. (a) Intact; (b) σ_3 = 2 MPa; (c) σ_3 = 5 MPa; (d) σ_3 = 10 MPa; (e) σ_3 = 20 MPa.

5. Conclusions

Laboratory physical model of granite with a circular hole is simulated numerically with the PFC2D code. The macroscopic fracture propagation and failure pattern of the BPM are in close agreement with laboratory observations. The different diameters of the hole revealed the importance of size for the underground openings. BPMs with two pre-existing holes have relative fracture propagation and failure patterns. Biaxial tests revealed differences in fracture mechanisms observed in comparison with UCS tests, and these differences become more significant as the lateral stress is augmented. Further investigation is required for the micro-mechanisms leading to damage accumulation and fracture around large-scale openings in compression.

REFERENCES

Carter BJ, Lajtai EZ, Petukhov A (1991). Primary and remote fracture around underground cavities. *International Journal for Numerical and Analytical Methods in Geomechanics*, 15(1), 21-40.

Itasca Consulting Group Inc (2014). PFC 5.0 Documentation.

Lajtai EZ (1971). A theoretical and experimental evaluation of the Griffith theory of brittle fracture. *Tectonophysics*, 11, 129-156.

Lotidis MA (2014). The Approach of Synthetic Rock Mass for the Numerical Simulation of the Brittle Rocks' Failure around Underground Openings. *Diploma Thesis*, School of Mining and Metallurgical Engineering NTUA, Athens, Greece.

Lotidis MA, Nomikos PP, Sofianos AI (2015). A numerical investigation of rock fracture around cavities in compression. *Proceedings of Eurock 2015: Future Development of Rock Mechanics*, Salzburg, Austria, 719-724.

Potyondy DO, Cundall PA (2004). A bonded-particle model for rock. *International Journal of Rock Mechanics and Mining Sciences*, 41, 1329-1364.

Potyondy DO (2012). A flat-jointed bonded-particle material for hard rock. *Proceedings of the 46th US Rock Mechanics Symposium*, Chicago, USA, paper ARMA 12-501.